A Study of Roll Vortices in the Atmospheric Boundary Layer

Andreas Chlond

Max-Planck-Institut für Meteorologie, Hamburg

(Manuscript received 04.04.1984, in revised form 10.09.1984)

Abstract:
The dynamics of two-dimensional, dynamically forced roll vortices is investigated in the neutral atmospheric boundary layer by use of a four-component spectral model.

Although the truncated model of shear flow cannot be expected to describe the developing structure in detail, information is given about the critical points at which the character of the flow is expected to change.

The study consists of finding constant equilibrium solutions and then conducting a linearized analysis to determine their stability with respect to small disturbances. In addition, numerical integrations of the phase space trajectories of the solutions were performed to reveal the existence of temporally periodic solutions for a certain range of the external parameters.

Finally, the calculated roll-scale transports of lateral momentum are compared with observational data.

Zusammenfassung: Eine Studie über Wirbelrollen in der atmosphärischen Grenzschicht
Die Dynamik zweidimensionaler, dynamisch erzeugter Wirbelrollen wird in der neutralen atmosphärischen Grenzschicht mit Hilfe eines vierkomponentigen spektralen Modells untersucht.

Obwohl nicht erwartet werden darf, daß das niederspektrale Modell der Scherströmung exakt die sich entwickelnde Strömungskonfiguration vorhersagt, kann dennoch Auskunft über die kritischen Parameterwerte gegeben werden, an denen eine Änderung im Charakter der Strömung zu erwarten ist.

In der Studie werden zunächst die stationären Gleichgewichtslösungen des Modells ermittelt und ihre Stabilität mit Hilfe einer linearen Störungsanalyse überprüft. Zusätzlich werden numerisch ermittelte Lösungen der Gleichungen angegeben, um die Existenz zeitlich periodischer Lösungen für bestimmte Parameterbereiche nachzuweisen.

Schließlich werden die berechneten Vertikaltransporte von lateralem Impuls in der Rollenskala mit Meßdaten verglichen.

Résumé: Une étude des tourbillons en rouleaux dans la couche limite atmosphérique
On étudie, à l'aide d'un modèle spectral à quatre composantes, la dynamique de tourbillons en rouleaux à deux dimensions, engendrés dynamiquement, dans la couche limite atmosphérique neutre. Bien qu'on ne puisse pas attendre, en raison du cisaillement tronqué, que le modèle décrive en détail la configuration du développement, on obtient de l'information sur les points critiques où le caractère de l'écoulement est susceptible du changer.

L'étude consiste à trouver les solutions stationnaires d'équilibre et à effectuer alors une analyse linéarisée pour déterminer leur stabilité vis-à-vis de petites perturbations. En outre, on a réalisé des intégrations numériques des trajectoires des solutions dans l'espace de phase, en vue de révéler l'existence de solutions périodiques pour une certaine gamme des paramètres externes. Finalement, on a comparé avec des données d'observation les transports verticaux calculés d'impulsion latérale à l'échelle des rouleaux.

0005-8173/85/01 0017–14 $ 03.00/0

1 Introduction

There exists ample observational evidence, for instance due to the KonTur experiment, that the dynamic state of the atmospheric boundary layer is often characterized by the presence of coherent motions, whose amplitudes are significant and at scales comparable to the thickness of the atmospheric boundary layer.

When the wind is suffenciently high and the heat flux not too strong, longitudinal roll vortices aligned approximately parallel to the mean wind seem to be the most obvious manifestation of organized convection.

The rolls under discussion here are the result of a dynamic shear instability, in contrast to convective rolls associated with a strongly unstable boundary layer with streamwise shear. Several experimental and theoretical studies have revealed the existence and nature of a shearing instability in the boundary layer and found that the mechanism of instability is associated with a point of inflection in the profile of velocity perpendicular to the rolls (e.g. KAYLOR and FALLER, 1966; LILLY, 1966; BROWN, 1970 and 1980; ETLING and WIPPERMANN, 1975).

In order to get more insight into some of the nonlinear aspects of the secondary flow in the neutral Ekman-layer, we study a low-order-spectral model of two-dimensional convection in presence of a mean wind component orthogonal to the rolls.

We adopt the philosophy proposed by LORENZ (1960, 1963) that essential aspects of the physics of complex hydrodynamical systems are revealed by models that are simplified to the point containing the nonlinearity in its most basic manifestation. We use the observed fact that under convective conditions the flow is dominated by a few spatial harmonics and cut-off the representation after four terms. In the study only nonlinear interactions between the mean flow and the secondary flow are included and interactions among the eddy terms are ignored. Such simplified models are often considered to incorporate the essential features of the nonlinear interactions and are of course simpler to analyse than the fully nonlinear system. The most striking consequence of the nonlinearity of the problem is that the nature of the solutions can change as the parameters of the problem are varied. Most significantly, stable solutions become unstable and there are combinations of parameters for which multiple solutions appear.

In Section 2 we present the basic equations and the Fourierrepresentation for the flow. In Sections 3 and 4 the steady-state solutions of the system and their stability depending on the external parameters are examined while Section 5 contains the results of the numerical time integrations. In Section 6 we compare our qualitative results with measurements reported by BRÜMMER et al. (1984).

2 Governing Equations

To simplify the problem we assume that all motions are parallel to the y-z-plane and no variations occur in the direction of the x-axis, which is in line with the roll axis. This assumption is equivalent to the requirement of two-dimensional disturbances, which realize only the shear in the plane perpendicular to their axis.

Starting point of the analysis are the continuity equation and the two equations of motion for an incompressible, neutrally buoyant, conservative fluid. By cross differentiating the equations of motion and introducing a streamfunction ψ, the vorticity equation of the problem is obtained.

$$v = -\frac{\partial \psi}{\partial z} \qquad w = \frac{\partial \psi}{\partial y}$$

$$\frac{\partial}{\partial t} \nabla^2 \psi + J(\psi, \nabla^2 \psi) = 0 \tag{1}$$

Here $\nabla^2 \psi$ represents the vorticity of the motions in the plane normal to the horizontal axis of the vortices and the Jacobian operator is defined as

$$J(a, b) = \frac{\partial a}{\partial y}\frac{\partial b}{\partial z} - \frac{\partial a}{\partial z}\frac{\partial b}{\partial y}.$$

To represent the effects of the small scale turbulence, a constant eddy diffusivity coefficient K_m is used. The processes, which set up a mean lateral velocity profile are not explicitly included in the model. With respect to this production of energy it is assumed that all mechanisms involved could be interpreted as a time independent forcing field $\tilde{\psi}$, which has to be determined by observational data. For simplicity the time scales of the forcing and of the diffusive processes are assumed to be the same. The model is then specified by

$$\frac{\partial}{\partial t}\nabla^2 \psi + J(\psi, \nabla^2 \psi) = K_m \nabla^4 (\psi - \tilde{\psi}). \tag{2}$$

It is convenient to nondimensionalize the equations, using the convection layer depth H and the R.M.S. value of the forcing velocity $\tilde{v}_\sigma$ as characteristic velocity and height scale so that we can rewrite the variables of the problem in terms of nondimensional variables to be denoted by an asterisk as follows

$$y = H \cdot y^* \qquad t = \frac{H}{\tilde{v}_\sigma} \cdot t^*$$

$$z = H \cdot z^* \qquad \psi = \tilde{v}_\sigma \cdot H \cdot \psi^*$$

$$\tilde{v}_\sigma = \left(\frac{1}{H} \int_0^H \left(\frac{\partial \tilde{\psi}}{\partial z} \right)^2 dz \right)^{1/2}.$$

By introduction of these transformations in Equation (1), we obtain the vorticity equation in nondimensional form, containing the turbulent Reynoldsnumber Re as a nondimensional parameter.

$$\frac{\partial}{\partial t^*}\nabla^{*2} \psi^* + J^*(\psi^*, \nabla^{*2} \psi^*) = Re^{-1} \nabla^{*4} (\psi^* - \tilde{\psi}^*)$$

$$Re = \frac{\tilde{v}_\sigma \cdot H}{K_m}. \tag{3}$$

We shall apply the vorticity equation to a flow confined between two surfaces and assume that ψ^* is periodic in the y-direction. The problem is most tractable, if free slip boundary conditions are adopted. In this case ψ^* and $\nabla^{*2} \psi^*$ vanish at both horizontal boundaries.

$$\psi^* = \nabla^{*2} \psi^* = 0 \quad \text{for} \quad \begin{cases} z^* = 0 \\ z^* = 1. \end{cases}$$

With respect to atmospheric applications the no-slip boundary condition at the lower border would be more realistic. But for simplicity we make no attempt to incorporate this condition, because in most respects the results may differ only quantitatively when the fluid is forced to be motionless at the lower boundary.

To obtain a solution of the vorticity equation, which gives insight into the complicated forms of nonlinearity, the spectral method is applied. The flow field is represented as a double Fourier-series according to

$$\psi^*(y^*, z^*, t^*) = \sum_{\underline{k}} a_{\underline{k}}(t^*) \cdot e^{i\underline{k} \cdot \underline{x}} \qquad \tilde{\psi}^*(y^*, z^*) = \sum_{\underline{k}} \tilde{a}_{\underline{k}} \cdot e^{i\underline{k} \cdot \underline{x}}$$

With vector $\underline{x}$ and the wavenumber vector $\underline{k}$

$$\underline{x} = (y^*, z^*)$$

$$\underline{k} = (k_n, l_m) = \left(\frac{2 \cdot \pi}{L/H} \cdot n, \frac{2 \cdot \pi}{2} \cdot m\right).$$

Where m and n are integers representing the horizontal and vertical Fourier mode numbers and L/H, 2 are the fundamental wavelengths in the y*-direction and in the z*-direction, respectively.

The infinite set of ordinary differential equations governing the time variations of the Fourier-coefficients for the motion are formally obtained via Fourier-transformation of the vorticity equation.

$$|\underline{l}|^2 \dot{a}_{\underline{l}} + \sum_{\underline{p},\underline{q}} C_{\underline{l}}^{\underline{p},\underline{q}} a_{\underline{p}} \cdot a_{\underline{q}} = -\mathrm{Re}^{-1} |\underline{l}|^4 (a_{\underline{l}} - \tilde{a}_{\underline{l}}) \tag{4}$$

$$C_{\underline{l}}^{\underline{p}\,\underline{q}} = \begin{cases} (|\underline{p}|^2 - |\underline{q}|^2) \cdot (p_y \cdot q_z - p_z \cdot q_y) & \underline{p} + \underline{q} = \underline{l} \\ 0 & \text{otherwise} \end{cases}$$

Here the dot denotes a derivate with respect to the dimensionless time. Note that the quadratic terms represent nonlinear interactions among the spectral components of the motion field and the linear terms on the right hand side represent viscous damping and forcing, respectively. The interaction coefficient $C_{\underline{l}}^{\underline{p},\underline{q}}$ is non-zero, if the selection rule $\underline{l} = \underline{p} + \underline{q}$ is fullfilled.

In accordance with the remarks in the introduction we shall restrict our attention to a representation consisting of only a small number of modes. The highly truncated system is formed by retaining only four terms in the expansion of the streamfunction, with two variables representing the mean velocity profile and the other two representing the secondary flow.

Let

$$\psi^* = (2)^{-1/2} \cdot x_1 \cdot \sin(l \cdot z^*) + (2)^{-1/2} \cdot x_2 \cdot \sin(m \cdot z^*) + \\ + x_3 \cdot \cos(k_1 \cdot y^*) \cdot \sin(q \cdot z^*) + x_4 \cdot \sin(k_1 \cdot y^*) \cdot \sin(p \cdot z^*). \tag{5}$$

The forcing function is taken as

$$\tilde{\psi}^* = (2)^{-1/2} \tilde{x}_1 \cdot \sin(l \cdot z^*) + (2)^{-1/2} \tilde{x}_2 \cdot \sin(m \cdot z^*).$$

Introducing the shape-parameter $\theta = \mathrm{arctg}(m \cdot \tilde{x}_2 / l \cdot \tilde{x}_1)$, the forcing function can be rewritten as

$$\tilde{\psi}^* = (2)^{1/2} \cdot l^{-1} \cdot \cos\theta \cdot \sin(l \cdot z^*) + (2)^{1/2} \cdot m^{-1} \cdot \sin\theta \cdot \sin(m \cdot z^*)$$

since

$$\left(\frac{\tilde{x}_1^2 l^2}{4} + \frac{\tilde{x}_2^2 \cdot m^2}{4}\right)^{1/2} = 1.$$

In Equation (5) the first two terms on the right are independent of y* and therefore represent the mean velocity profile. The vertical wavenumbers are choosen to be $l = \pi$ and $m = 3\pi$.

The remaining terms represent the secondary flow disturbances with the horizontal wavenumber $k_1 = 2\pi/L/H$. In order that they may interact with the mean flow their vertical wavenumbers p and q must satisfy the selection rules $m = p + q$ and $l = p - q$, which require $p = 2 \cdot \pi$ and $q = \pi$. Together they describe a wave of a single horizontal wavenumber, but a variable shape and a variable phase. Because there are so few degrees of freedom, the shape of the wave depends upon the phase, so that the model cannot picture the motion of disturbances without change of shape.

The governing equations of the truncated model are obtained either from the universal spectral vorticity equation (4), or by substituting Equation (5) directly into Equation (3).

The four-coefficient model is now specified on the domain $0 \leqslant y^* \leqslant L/H$, $0 \leqslant z^* \leqslant 1$ by

$$\pi^2 \cdot \dot{x}_1 = \Gamma_{x_1}^{x_3, x_4} \cdot x_3 \cdot x_4 - \mathrm{Re}^{-1} \cdot \pi^4 \left(x_1 - \frac{2 \cdot \cos\theta}{\pi \chi} \right) \tag{6}$$

$$9\pi^2 \cdot \dot{x}_2 = + \Gamma_{x_2}^{x_3, x_4} \cdot x_3 \cdot x_4 - \mathrm{Re}^{-1} \cdot 81 \cdot \pi^4 \cdot \left(x_2 - \frac{2 \sin\theta}{3 \cdot \pi} \right) \tag{7}$$

$$(k_1^2 + \pi^2) \cdot \dot{x}_3 = \Gamma_{x_3}^{x_1, x_4} \cdot x_1 \cdot x_4 + \Gamma_{x_3}^{x_2, x_4} \cdot x_2 \cdot x_4 - \mathrm{Re}^{-1} \cdot (k_1^2 + \pi^2)^2 \cdot x_3 \tag{8}$$

$$(k_1^2 + 4 \cdot \pi^2) \dot{x}_4 = \Gamma_{x_4}^{x_1, x_3} \cdot x_1 \cdot x_3 + \Gamma_{x_4}^{x_2 \cdot x_3} \cdot x_2 \cdot x_3 - \mathrm{Re}^{-1} \cdot (k_1^2 + 4 \cdot \pi^2)^2 \cdot x_4 . \tag{9}$$

Where

$$\Gamma_{x_1}^{x_3, x_4} = -\frac{3\pi^3 \cdot k_1}{2 \cdot \sqrt{2}} \qquad \Gamma_{x_2}^{x_3, x_4} = \frac{9\pi^3 \cdot k_1}{2\sqrt{2}}$$

$$\Gamma_{x_3}^{x_1, x_4} = \frac{3\pi^3 \cdot k_1 + k_1^3 \cdot \pi}{2 \cdot \sqrt{2}} \qquad \Gamma_{x_3}^{x_2, x_4} = \frac{-3\pi k_1^3 + 15\pi^3 \cdot k_1}{2 \cdot \sqrt{2}}$$

$$\Gamma_{x_4}^{x_1, x_3} = -\frac{k_1^3 \cdot \pi}{2 \cdot \sqrt{2}} \qquad \Gamma_{x_4}^{x_2, x_3} = \frac{3\pi k_1^3 - 24\pi^3 k_1}{2 \cdot \sqrt{2}} .$$

Under Equations (6)–(9) two integral quantities, namely the mean kinetic energy E

$$E = \frac{1}{8} (\pi^2 \cdot x_1^2 + 9 \cdot \pi^2 \cdot x_2^2 + (k_1^2 + \pi^2) \cdot x_3^2 + (k_1^2 + 4\pi^2) \cdot x_4^2)$$

and the mean square vorticity V

$$V = \frac{1}{8} (\pi^4 \cdot x_1^2 + 81 \cdot \pi^4 \cdot x_2^2 + (k_1^2 + \pi^2)^2 \cdot x_3^2 + (k_1^2 + 4\pi^2)^2 \cdot x_4^2)$$

are readly seen to be conserved in the limit $\mathrm{Re} \to \infty$.

The simple system may seem to be a rather crude approximation of a hydrodynamical system, it can however picture the nonlinear interaction between the mean flow and the superposed disturbances.

To study the growth of intensity of the roll vortices, the initial conditions consist of the basic mean velocity profile plus a infinitesimal disturbance in the component x_3. Thus we choose

$$x_1 = \frac{2 \cdot \cos\theta}{\pi} \quad x_2 = \frac{2 \cdot \sin\theta}{3 \cdot \pi} \quad x_3 = \epsilon \quad x_4 = 0 \quad |\epsilon| \ll 1.$$

Figure 1 shows some of the investigated mean velocity profiles as function of the shape-parameter θ. This parameter could be regarded as a measure of steepness of the inflection point, that is, so the smaller the value of the shape-parameter, the greater is the vorticity of the mean velocity profile at $z^* = 0.5$. There are obviously two additional i.-points between $z^* = .5$ and the boundaries, if $\theta < 174°$, but the magnitude of the velocity gradient at these points is surely much smaller than at $z^* = 0.5$. Thus, only the inflection point at $z^* = 0.5$ is likely to have measureable significance. In the atmospheric boundary layer, whose mean flow is produced by a balance of viscous-, coriolis- and pressure forces, two dimensional velocity profiles (Ekman spirals) may develop with inflection points in the lateral wind component (see Figure 16 in the paper of LILLY, 1966). These profiles exhibit some similarities to those used in the model, but, on the other hand, the profiles used in the model seem to be arbitrary in some way, since the heigth of the inflection point and the corresponding velocity in this point are fixed. Nevertheless, we think that these restrictions do not affect essential aspects for the understanding of boundary layer roll phenomena.

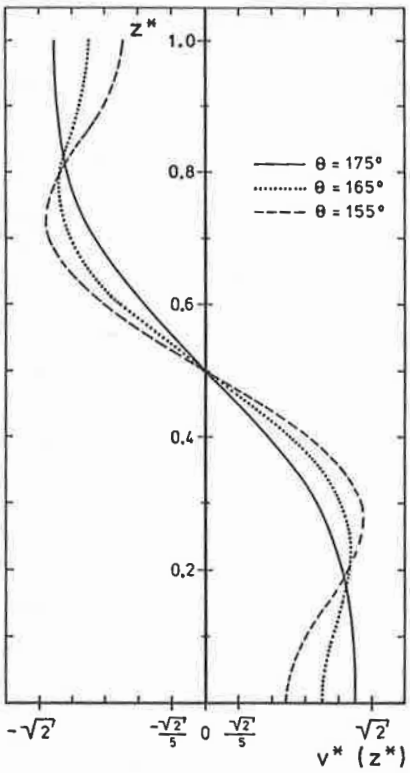

Fig. 1
Investigated mean velocity profiles for different values of the shape-parameter θ.

In the next sections we will examine the solutions and their stability as functions of the Reynoldsnumber Re, the domain aspect ratio L/H and the shape-parameter θ. In this way we can investigate how the roll circulation will develop in response to different mean velocity profiles.

3 Stationary Solutions and their Stability

The stationary solutions are a crucial subclass of solutions to the spectral system. They can be determined analytically as an algebraic function of the model parameters Re, L/H and θ. Besides their intrinsinc value, the stationary solutions are the foundation for the investigation of the asymptotic properties of the temporally varying solutions of Equations (6)–(9).

For the steady state time derivates vanish and from Equations (6)–(9) we can write

$$0 = \Gamma_{x_1}^{x_3,x_4} \cdot x_3 \cdot x_4 - \mathrm{Re}^{-1} \cdot \pi^4 \cdot \left(x_1 - \frac{2 \cdot \cos\theta}{\pi} \right) \tag{10}$$

$$0 = \Gamma_{x_2}^{x_3,x_4} \cdot x_3 \cdot x_4 - \mathrm{Re}^{-1} \cdot 81 \cdot \pi^4 \cdot \left(x_2 - \frac{2 \cdot \sin\theta}{3\pi} \right) \tag{11}$$

$$0 = \Gamma_{x_3}^{x_1,x_4} \cdot x_1 \cdot x_4 + \Gamma_{x_3}^{x_2,x_4} \cdot x_2 \cdot x_4 - \mathrm{Re}^{-1} \cdot (k_1^2 + \pi^2)^2 \cdot x_3 \tag{12}$$

$$0 = \Gamma_{x_4}^{x_1,x_3} \cdot x_1 \cdot x_3 + \Gamma_{x_4}^{x_2,x_3} \cdot x_2 \cdot x_3 - \mathrm{Re}^{-1} \cdot (k_1^2 + 4\pi^2)^2 \cdot x_4 . \tag{13}$$

By eliminating x_1, x_2 and x_4 from Equations (10)–(13) we derive a fifth degree polynomial in x_3

$$x_3^5 + \lambda_1 \cdot x_3^3 + \lambda_2 \cdot x_3 = 0 \tag{14}$$

that governs the stationary solutions. The coefficients λ_i are functions of the Reynoldsnumber Re, the shape-parameter θ and the domain aspect ratio L/H and are listed in the Appendix. Since the coefficients are real, complex roots must occur in conjugate pairs. Hence, there is always at least one real root for Equation (14) and may be more depending on the parameter values λ_1 and λ_2. The solutions are easily calculated from Equations (14) and (10)–(13), and the expression for the first is

$$x_1^s = \frac{2 \cdot \cos\theta}{\pi} \quad x_2^s = \frac{2 \cdot \sin\theta}{3 \cdot \pi} \quad x_3^s = 0 \quad x_4^s = 0. \tag{15}$$

The solution (15) will be called the S_1 trivial branch, because it corresponds to the undisturbed basic state consisting of the initial mean velocity profile and vanishing amplitudes of the coefficients describing the secondary flow. It is clear from Equations (10)–(13) that this configuration is always a solution. But when λ_2 is forced to negative values, additional solutions emerge, branching off from the basic solution. We obtain

$$\begin{aligned}
x_1^s &= \frac{2 \cdot \cos\theta}{\pi} - \frac{3 \cdot \mathrm{Re} \cdot k_1}{2 \cdot \sqrt{2} \cdot \pi} \cdot x_3^s \cdot x_4^s \\
x_2^s &= \frac{2 \cdot \sin\theta}{3 \cdot \pi} + \frac{\mathrm{Re} \cdot k_1}{18 \cdot \sqrt{2} \cdot \pi} \cdot x_3^s \cdot x_4^s \qquad (16) \\
x_3^s &= \pm \left(-\frac{\lambda_1}{2} + \left(\frac{\lambda_1^2}{4} - \lambda_2 \right)^{1/2} \right)^{1/2} \qquad (16) \\
x_4^s &= -\frac{C_4 \cdot x_3^s}{(C_5 + C_6 \cdot (x_3^s)^2)}
\end{aligned}$$

for the c_i defined in the Appendix.

Note that two more solutions (corresponding to the plus or minus sign in Equation (16)) appear, which will be called the S_2 and S_2^* primary branches. These solutions are physically equivalent differing only in phase by 180° and correspond to nontrivial steady states of convection in which the finite amplitude roll circulation coexists with a modified mean flow. We will discuss the implication of the bifurcation and stability of these stationary solutions in Section 4.

4 Stability and Bifurcation Properties

In this section we examine the stability properties of the stationary solutions with respect to infinitesimal disturbances.

We have seen that nonlinear differential equations such as those that govern the present mathematical model of inflection point instability usually have multiple solutions for some values of the controling parameters. The critical values of the external parameters at which two or more solutions coalesce are called bifurcation points. Although bifurcation arises from nonlinearity, the stability characteristics of the solutions can be determined from the linearized form of Equations (6)–(9). Because one solution looses its stability at the bifurcation point, the two concepts of bifurcation and stability are intimately related. Thus, in order to discover the physically realizable configurations, we study the linearized equations in the neighborhood of the bifurcation points.

Denoting the stationary solution by $\underline{A} = (x_1^s, x_2^s, x_3^s, x_4^s)$ and the perturbations by $\underline{\alpha} = (x_1', x_2', x_3', x_4')$ we derive from Equations (6)–(9) the perturbation equations by ignoring products of perturbations. If the linear matrix operator is denoted by $\underline{\underline{L}}_A$ the linearized equation is now

$$\dot{\underline{\alpha}} + \underline{\underline{L}}_A(\underline{\alpha}) = 0 \tag{17}$$

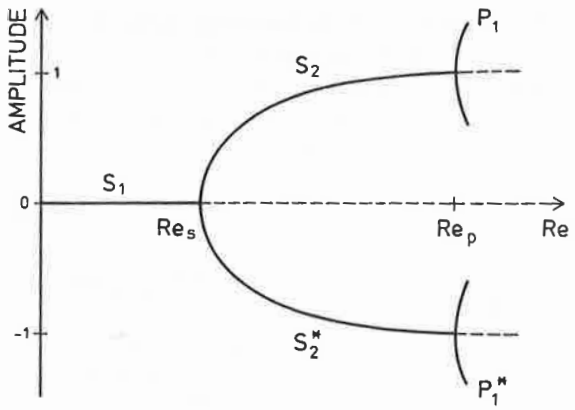

● **Fig. 2**
Schematic bifurcation diagram. Three steady branches S_1, S_2, S_2^* and two periodic solutions P_1, P_1^* are shown. For $Re < Re_s$ one steady solution S_1 exists, which corresponds to the basic state. S_1 looses its stability at $Re = Re_s$ but two other steady solutions S_2 and S_2^* emanate from this bifurcation point. S_2 and S_2^* are stable in the Reynoldsnumber intervall $Re_s < Re < Re_p$, but at $Re = Re_p$ these solutions exchange stability via Hopf bifurcation with periodic solutions P_1 and P_1^*.

Since Equation (17) has solutions of the form $\underline{\alpha}(t^*) = \hat{\underline{\alpha}} \exp(\sigma \cdot t^*)$, we obtain the characteristic equation

$$\sigma^4 + q_3 \cdot \sigma^3 + q_2 \cdot \sigma^2 + q_1 \cdot \sigma + q_0 = 0$$
$$\sigma = \sigma_R + i \cdot \sigma_i \qquad (18)$$

where the q_i are functions of Re, θ, L/H and $\underline{A}$. Hence, a time independent solution $\underline{A}$ will become unstable, if the real part of one eigenvalue σ passes through zero as the magnitude of a parameter is varied. Whenever the imaginary part of σ also vanishes at a critical point, then other steady solutions are expected to emanate from the stationary solution. If two eigenvalues cross the imaginary axis as a conjugate pair a Hopf bifurcation to a periodic solution is expected (SHIRER and WELLS, 1983).

Direct numerical solutions of Equation (18) yield the following results, which are summarized by means of a bifurcation diagram and are sketched in Figure 2.

The coordinates are the Reynoldsnumber and any Fourier-amplitude of the secondary circulation (scales are arbitrary). The trivial branch (see Equation (15)), labeled by S_1, lies on the abscissa; the primary branches (see Equation (16)) that bifurcate from it are denoted by S_2 and S_2^* and the suspected periodic solutions are identified by P_1 and P_1^*. Full lines are used to denote the stable portions of the solutions.

In Figure 2, the basic solution S_1 looses its stability at $Re = Re_s$, but two other solutions S_2 and S_2^* corresponding to the steady state of roll circulation emanate from this bifurcation point. The solutions S_2 and S_2^* are stable in the Reynoldsnumber interval $Re_s < Re < Re_p$, but at $Re = Re_p$ these solutions exchange stability via Hopf bifurcation with periodic solutions P_1 and P_1^*.

The physical explanation leading to the branching hierarchy in our model of shear flow lies in the inability of a slightly viscid fluid to maintain local extremes in vorticity of the mean flow profile. If the frictional forces are not strong enough to support these local strains in the fluid, the flow becomes unstable to small perturbations. The fluid develops waves to relieve the vorticity maximum at $z^* = .5$. The unstable perturbations equilibrate at some finite value, wherein the energy drawn from the mean flow exactly balances the secondary dissipation. In addition, the finite amplitude disturbances tend to alter the dynamically unstable mean flow profile so that it becomes stable in combination with the secondary flow. Finally, a transition to a temporally periodic changing flow pattern is possible, if the ratio of inertial to frictional forces exceeds a certain value. In this case oscillatory time variations of the perturbation kinetic energy and the mean flow kinetic energy will be observed excited by a cyclic interchange of energy between the mean flow and the secondary flow.

Apparently the inflection point instability mechanism due to the two other inflection points is filtered by the restriction to only two vertical wavenumbers in the representation of the secondary circulation,

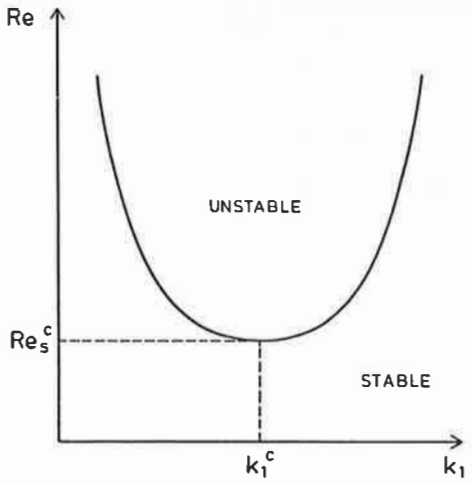

● **Fig. 3**
Schematic sketch of the neutral curve for the stability of the basic state to infinitesimal disturbances for a fixed value of the shape-parameter θ. The critical values of the Reynoldsnumber and the horizontal wavenumber are denoted by Re_s^c and k_1^c, respectively.

additional harmonics would be needed in order to capature the effect of the other inflection points and hence give rise to additional roll modes.

The numerical values of the Reynoldsnumber Re_s and Re_p at which branching occurs are functions of the parameters θ and L/H. Figure 3 gives a typical example of a stability diagram in which Re is plotted against the horizontal wavenumber $k_1 = 2\pi/L/H$. The point, which gives the minimum value of Re on the neutral curve is called the critical point. The Reynoldsnumber and wavenumber corresponding to the critical point are called the critical Reynoldsnumber Re_s^c and the critical wavenumber k_1^c, respectively. In order to reduce the number of external parameters in our problem, the horizontal wavenumber k_1 will hereafter be choosen to be equal to k_1^c.

The dependence of the critical Reynoldsnumber Re_s^c and the critical wavenumber k_1^c as function of the shape-parameter θ is illustrated in Figure 4. It is seen that Re_s^c (k_1^c) decreases (increases) with decreasing values of the shape-parameter θ; that is, so the steeper the inflection point, the sooner branching occurs and the smaller is the horizontal scale of the roll circulation.

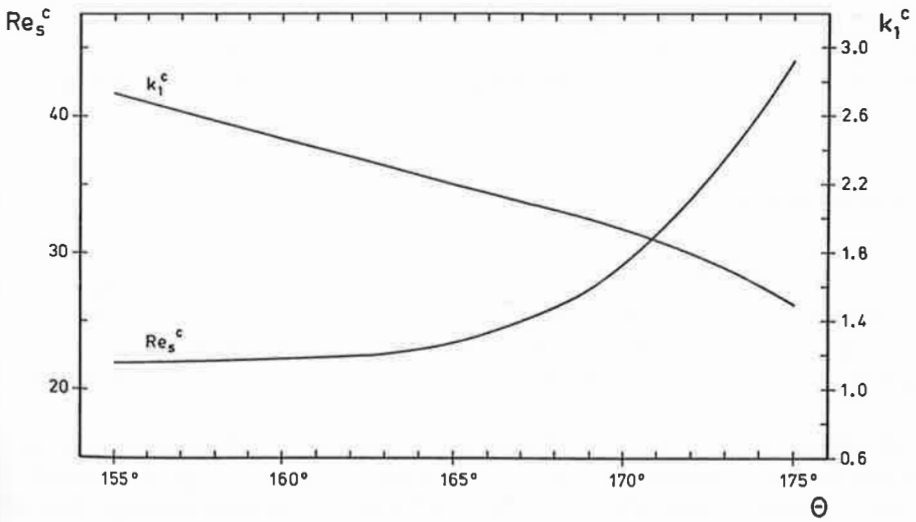

● **Fig. 4** Critical Renoldsnumber Re_s^c and critical wavenumber k_1^c versus shape-parameter θ.

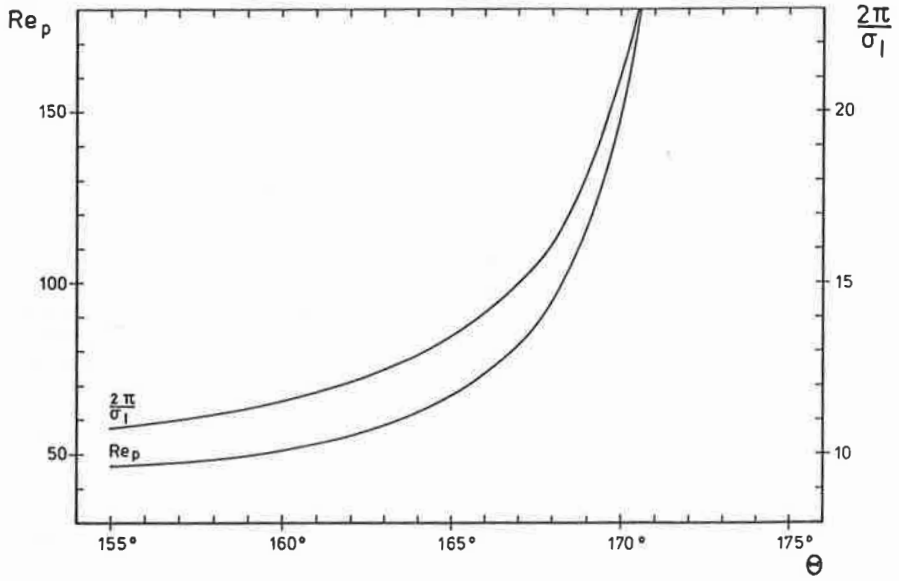

Fig. 5 The Reynoldsnumber Re_p at which Hopf bifurcation occurs and the expected period $2\pi/\sigma_i$ of the periodic solution as function of the shape-parameter θ.

The dependence of the Reynoldsnumber Re_p and the period $2\pi/\sigma_i$ of the expected periodic solutions corresponding to this Reynoldsnumber is given in Figure 5. Similar as in the case before Re_p is monotonously decreasing with decreasing values of θ; the periods of the periodic solutions show also this behaviour. Periodic solutions exist also for $\theta > 170°$, but the values of the Reynoldsnumber Re_p at which branching occurs and the corresponding period $2\pi/\sigma_i$ are out of the range to be plotted. From the non-dimensionalisation in the present model we note that the dimensional period T is given by $T = \frac{2\pi}{\sigma_i} \cdot \frac{H}{\tilde{v}_\sigma}$. For typical atmospheric conditions with $\tilde{v}_\sigma = 1\,m/s$ and $H = 1000\,m$ the non-dimensional period $2\pi/\sigma_i = 15$ corresponds to a dimensional period of approximately 4 hours. Thus, a temporally periodic changing flow pattern may be realized in the atmosphere, since the predicted periods of the oscillations are short compared to the intervall of time in which steady external conditions could be expected.

5 Numerical Integrations

To obtain numerical solutions of the system of Equations (6)–(9), numerical values for the external parameters must be specified. We shall let $\theta = 160°$ so that $k_i^c = 2.45$, $Re_s^c = 22$ and $Re_p = 51$ (see Figures 4 and 5). Since the behavior of the system in the vincinity of the branching points is of special interest, we choose supercritical values of Re with respect to Re_s^c and Re_p, respectively. For initial conditions we have choosen a slight departure from the basic state and of the state of steady convection, respectively.

A geometrical interpretation of the time dependent dynamics of the system could be given in the phase space, which is set up by the four variables (x_1, x_2, x_3, x_4). The trajectories were derived by numerical integration of the time dependent system of Equations (6)–(9) by use of the Euler-backward time integration scheme.

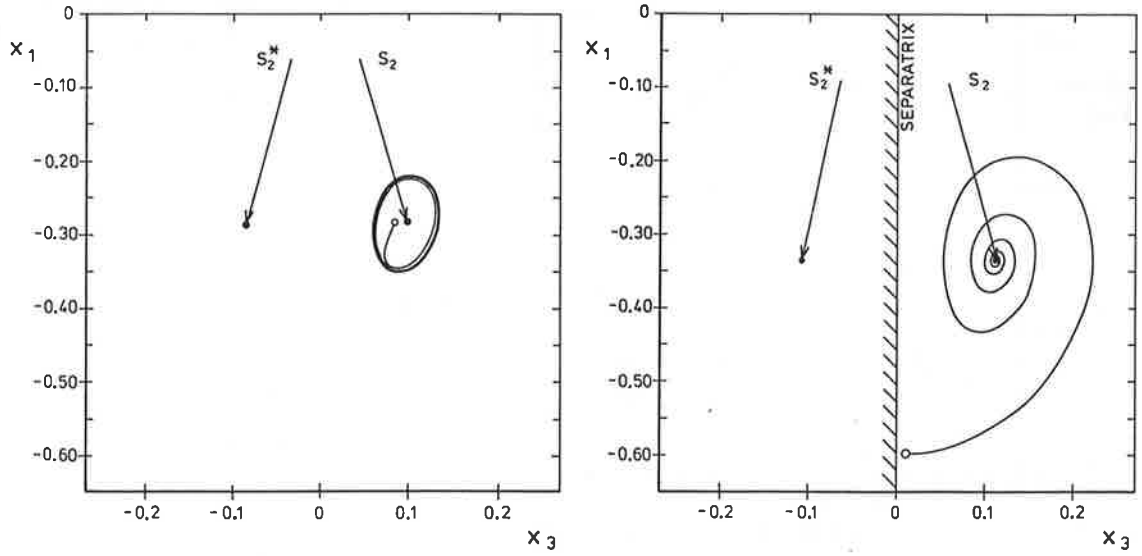

- **Fig. 6a** Projection of the four-dimensional trajectory into the $x_1 - x_3$ phase plane. The trajectory was obtained by numerical integration of Equations (6)–(9) with $\theta = 160°$, Re = 40. Initial conditions are denoted by an open circle, while stationary points are indicated by dots. The position of the Separatrix is also given.

- **Fig. 6b** As in Figure 6a except Re = 52. The figure displays the behavior of the system as it settles into the limit cycle.

In Figures 6a and 6b the four-dimensional trajectories are depicted by showing the projections in the $(x_1 - x_3)$ phase plane. This initial condition is indicated by an open circle and the arrowheads point at the positions of the projections of the stationary solutions S_2 and S_2^* marked with dots. The trajectories choosen for illustration in the pictures are representative of numerous trajectories obtained for other initial conditions.

In Figure 6a a phase plane representation of the transient behaviour of the four-variable system as it settles to the stationary solution S_2 is given. The trajectory spirals into S_2, which is called a stable focus, since all trajectories in its sourrounding were attracted. This behaviour is characteristic for all cases in the parameter range $Re_s^c < Re < Re_p$. In the middle of the picture the projection of the Separatrix is seen, which separates the basins of attraction of the both attractors.

The topologic structure of the attractor will change, if the Reynoldsnumber is raised above Re_p. Figure 6b displays the behaviour of the system in the case in which periodic solutions may be aspected. The trajectory is apparently approaching a limit cycle and the apparent period is approximately $\frac{2\pi}{\sigma_i}$ (see Figure 5).

6 Comparison of Model Results with Measurements

Cloud street observations were performed on four days during the KonTur experiment, on September 18, 20, 26 and 28, 1981. In this section we will compare our qualitative results with measurements performed on September 20, 1981 reported by BRÜMMER et al. (1984).

The wind profile measured on September 20 is presented in Figure 7. Neglecting the details of wind fluctuations, the along-roll component (u_R) has approximately a triangular shape and the cross-roll component (v_R) a tangent like profile with an inflection point at about 850 m. This indicates the dynamic instability as a possible mechanism of roll generation, because the heating from below is small.

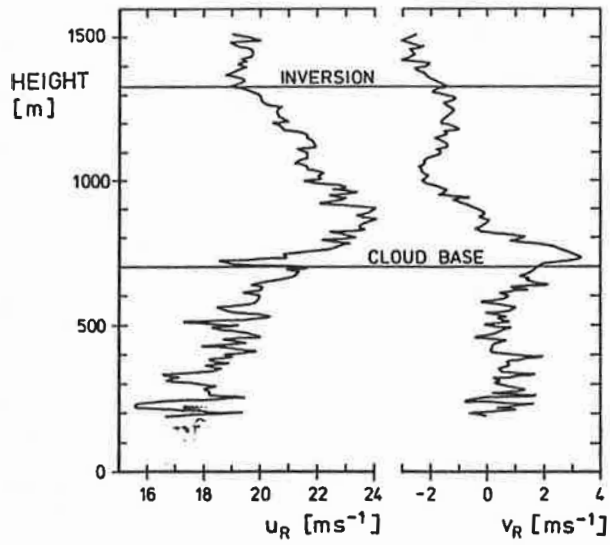

● **Fig. 7**
Mean wind components parallel (u_R) and normal (v_R) to roll orientation measured by the aircraft FALCON on September 20, 1981 (after BRÜMMER et al., 1984).

The sea surface was only 0.5 K warmer than the air. The horizontal wavelength of the boundary layer rolls was found to be about 3.1 times the convection layer depth H. Since the cloudy part of the roll circulation was observed to be rather small, we assume that the release of latent heat due to condensation was not essential to the formation of convective streets. Therefore a test of the model results against observational data may be justified.

To compare the measurements of roll-scale transports of cross-roll momentum with momentum transports derived from the model, we have to specify the values of the external parameters. We choose $\theta = 169°$ so that the corresponding horizontal wavelength $L/H = 2\pi/k_1^c$ is in accordance with the observed value. The scaling velocity $\tilde{v}_\sigma$ was estimated from the measured cross-roll wind profile to be $\tilde{v}_\sigma = 0.9$ m/s. The value H = 1300 m has been choosen for the height of the convection layer, which corresponds to the height of the inversion base. Finally, $K_m = 40\ m^2/s$ was jugded to be a realistic value for the momentum diffusion coefficient. The Reynoldsnumber Re = 30 belonging to this parameter constellation lies in the range $Re_s^c < Re < Re_p$ in which steady solutions exists (see Section 4).

Figure 8 shows the computed secondary flow pattern corresponding to the S_2 solution in the $y^* - z^*$ plane. The secondary flow consists of counterrotating skewed vortices, indicating energy transfer from the mean flow to the secondary circulation.

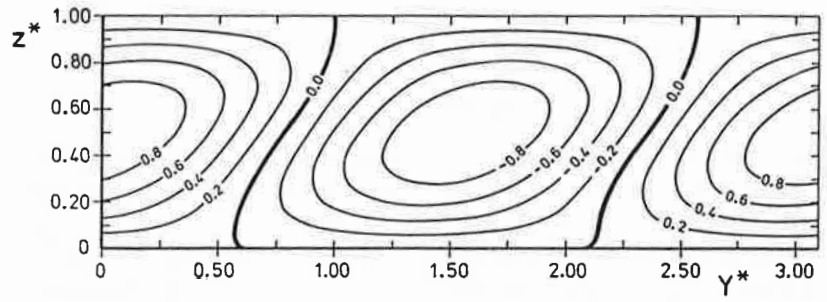

● **Fig. 8** Secondary flow pattern for an equilibrium finite amplitude circulation at $\theta = 169°$ and Re = 30. The streamlines correspond to counterrotating vortices.

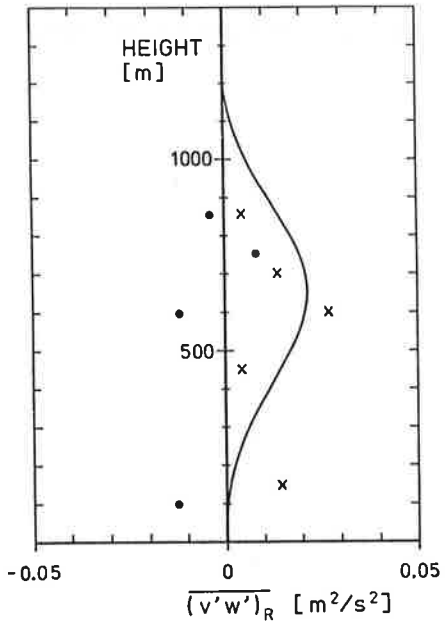

Fig. 9
Calculated and measured mean vertical roll-scale transports of cross-roll momentum as function of height. Calculations were performed for $\theta = 169°$, Re = 30. Data are marked with dots and crosses and refer to aircraft measurements from FALCON and HERCULES, respectively (After BRÜMMER et al., 1984).

The calculated and measured mean vertical roll-scale transports of cross-roll momentum as function of height are sketched in Figure 9. Data are marked with dots and crosses and refer to aircraft measurements from FALCON and HERCULES, respectively. The fluxes vanish at the boundaries and reach their maxima arround mid-levels, corresponding to the heigth of the inflection point, where the largest shear is present. The computed fluxes are not inconsistent with the observatational data, and we believe that the observations of cloud streets during the KonTur experiment could be explained with the inflection point instability mechanism.

7 Conclusions

The stationary and evolutionary solutions of a four-component spectral model designed to represent dynamically forced boundary layer rolls have been examined for the case in which the cross-roll mean flow interacts with smaller scale disturbances.

We have revealed the possibility of stationary and periodic solutions with varying stability domains of attraction or repulsion. Bifurcations occur in the model as the external parameters are modified.

When our results are tested against observatational data, qualitative agreement was obtained. Certainly, this agreement should not be overestimated, because of the highly restrictive model asumptions. It should be realized that our highly truncated spectral model could give only a poor description of a real fluid system with infinite many degrees of freedom. In addition, since the interaction between the velocity and thermal fields and the effects of condensational heating are completely neglected, it works best for rather confined fluids with "dry streets" where all modes of motion, except for a few selected ones, are highly damped.

Nevertheless, our results are encouraging for further work and we hope that this study provides a basis for further discussion to clarify our understanding of boundary layer roll phenomena.

Appendix

Derivation of the Polynominal Equation (14)

Combination of Equations (10) and (11) yields

$$x_1 = \frac{2 \cdot \cos\theta}{\pi} - \frac{3 \cdot Re \cdot k_1}{2\sqrt{2} \cdot \pi} \cdot x_3 \cdot x_4$$

$$x_2 = \frac{2 \cdot \sin\theta}{3 \cdot \pi} + \frac{Re \cdot k_1}{18 \cdot \sqrt{2} \cdot \pi} \cdot x_3 \cdot x_4$$

Inserting these expressions into Equations (12) and (13) gives

$$0 = C_1 \cdot x_4 + C_2 \cdot x_3 + C_3 \cdot x_3 \cdot x_4^2 \tag{A1}$$

$$0 = C_4 \cdot x_3 + C_5 \cdot x_4 + C_6 \cdot x_3^2 \cdot x_4 . \tag{A2}$$

Where $C_1 = 2k_1 \cdot \pi^2 \cdot (3 \cdot \cos\theta + \sin\theta) + 2 \cdot k_1^3 (\cos\theta - \sin\theta)$

$C_2 = -2 \cdot \sqrt{2} \cdot Re^{-1} (k_1^2 + \pi^2)^2$

$C_3 = -k_1^2 \cdot Re(5k_1^2 + 11\pi^2)/3 \cdot \sqrt{2}$

$C_4 = -(16k_1 \cdot \pi^2 \cdot \sin\theta + 2k_1^3(\cos\theta - \sin\theta))$

$C_5 = -2 \cdot \sqrt{2} \cdot Re^{-1} (k_1^2 + 4\pi^2)^2$

$C_6 = -k_1^2 \cdot Re \cdot (4\pi^2 - 5k_1^2)/3 \cdot \sqrt{2}.$

From Equation (A2) we obtain

$$x_4 = -\frac{C_4 \cdot x_3}{(C_5 + C_6 \cdot x_3^2)} . \tag{A3}$$

Finally, after inserting Equation (A3) into (A1), we get

$$0 = x_3^5 + \lambda_1 \cdot x_3^3 + \lambda_2 \cdot x_3 .$$

Where

$$\lambda_1 = \frac{(C_3 \cdot C_4^2 + (2 \cdot C_2 \cdot C_5 - C_1 \cdot C_4) \cdot C_6)}{C_2 \cdot C_6^2} \qquad \lambda_2 = \frac{(C_2 \cdot C_5 - C_1 \cdot C_4) \cdot C_5}{C_2 \cdot C_6^2} .$$

References

BROWN, R. A., 1970: A secondary flow model for the planetary boundary layer. J. Atmos. Sci. **27**, 742–757.

BROWN, R. A., 1980: Longitudinal instabilities and secondary flows in the planetary boundary layer: a rewiew. Rev. of Geophys. and Space Phys. **18**, 683–697.

BRÜMMER, B., S. BAKAN and H. HINZPETER, 1985: KonTur-observations of cloud streets and open cellular structures. Submitted to Dynamics of Oceans and Atmospheres.

ETLING, D. and F. WIPPERMANN, 1975: On the instability of a planetary boundary layer with Rossby number similarity. Boundary-Layer Meteorology **9**, 341–360.

FALLER, A. J. and R. E. KAYLOR, 1966: A numerical study of the instability of the laminar Ekman boundary layer. J. Atmos. Sci. **23**, 466–480.

LILLY, D. K., 1966: On the stability of Ekman boundary flow. J. Atmos. Sci. **23**, 481–494.

LORENZ, E. N., 1960: Maximum simplification of the dynamic equations. Tellus **12**, 243–254.

LORENZ, E. N., 1963: Deterministic nonperiodic flow. J. Atmos. Sci. **20**, 130–141.

SHIRER, N. H. and R. WELLS, 1983: Mathematical structure of the singularities of the transitions between steady states in hydrodynamic systems. Springer Verlag, 277 pp.